Journal of Applied Polymer Science

Enzymatic Degradation of Polylactide/Layered Silicate Nanocomposites: Effect of Organic Modifiers

Narendra K. Singh,[1] Biswa Pratim Das Purkayastha,[2] Muktikanta Panigrahi,[1] Rajeev K. Gautam,[1] Rathindra M. Banik,[3] Pralay Maiti[1]

[1]School of Materials Science and Technology, Institute of Technology, Banaras Hindu University, Varanasi 221 005, India
[2]Department of Zoology, Banaras Hindu University, Varanasi 221 005, India
[3]School of Biochemical Engineering, Institute of Technology, Banaras Hindu University, Varanasi 221 005, India

Correspondence to: P. Maiti (E-mail: pmaiti.mst@itbhu.ac.in)

ABSTRACT: Biodegradable polylactide (PLA)/layered silicate nanocomposites have been prepared via solution route using two different kinds of organically modified nanoclays. The nanostructure as observed from wide-angle X-ray diffraction indicates intercalated hybrids and the extent of intercalation depends on the type of organic modifiers used. Melt-quenched PLA and its nanocomposites are predominantly amorphous but, after annealing, they are fairly crystalline. The nanohybrids show significant improvement in thermal properties as compared to neat polymer. The nature of interaction between nanoclays and matrix polymer depends on the organic modifiers used, as evident from varying heat of fusion and shifting of Fourier transform infrared peaks. The nanoclays act as nucleating agent, and thereby, control the spherulite dimension of the matrix. The comparison of biodegradation of PLA and its nanocomposites has been studied in enzyme, compost, and buffer solution. Biodegradability of PLA has significantly been enhanced in the presence of nanoclays and the rate varies on organic modifications. The surface morphology, before and after enzymatic degradation, confirms the relative rate of degradation through laser scanning confocal images, scanning electron microscope, and atomic force microscope. © 2012 Wiley Periodicals, Inc. J. Appl. Polym. Sci. 000: 000–000, 2012

KEYWORDS: polylactide; nanocomposites; biodegradation; mechanical properties; morphology

Received 29 September 2010; accepted 23 April 2012; published online
DOI: 10.1002/app.37954

INTRODUCTION

Polylactide (PLA) is a biocompatible[1,2] and biodegradable polymer that has drawn significant interest in recent years because of its unique physical and mechanical properties, synthesized from renewable resources and readily biodegradable.[3–8] Biomedical and pharmaceutical applications of PLA range from sutures and tissue engineering to biologically active controlled release devices.[9,10] PLA can be synthesized via ring-opening polymerization of lactides or condensation polymerization of all stereoisomers of lactic acid monomer, which has three enantiomers, D, L, and meso forms, which are produced by fermentation of corn, potato, sugar, cane, and sugar beat among other plant resources.[11] However, slow crystallization and sluggish degradation rate have limited its wide applications that necessitate the use of polymer nanotechnology to improve the properties.

To overcome the aforementioned problems, the preparation of nanocomposites with organically modified layered silicate has come into picture by dispersing few weight percentages of nanoclays in polymer matrix.[12–20] The nanoparticles have advantages over its micrometer size counterpart as better interactions can be achieved through higher specific surface area of nanoparticles. In addition to the fact that organically modified surface can further induce the compatibility with polymer matrix. The main reason for these improved properties is interfacial interaction between polymer matrix and organically modified layered silicates. Okamoto's group first prepared PLA nanocomposites (PLACNs) via melt extrusion, which exhibit remarkable improvement of material properties such as dynamic mechanical properties (G' increases by 230% at 100°C as compared to pure PLA), crystallization behavior (faster crystallization kinetics in nanocomposites with respect to pyre PLA), gas permeability (oxygen gas permeability of nanocomposite becomes 144 from its value for pure PLA of 200 mL μm m^{-2} day^{-1} MPa^{-1}) and improved biodegradation in nanocomposites as compared to pristine PLA through CO_2 evaluation, molecular mass, and

Additional Supporting Information may be found in the online version of this article.

residual weight measurement in compost media.[21–25] The melt intercalation kinetics and morphological evolution as well as linear viscoelastic properties of PLACNs have been studied by Masuko's groups.[26,27] The effect of nanoclay on spherulitic texture,[26] biodegradation of PLA, and its nanocomposites with C18 nanoclay have been reported in detail.[28] In addition to these properties, the work on shape memory effect,[29] implants system, and drug delivery have also been reported.[30,31] Doi et al. reported the enzymatic degradation of pure PLA. The enzymatic degradation, its mechanism, as well as the effect of chain stereochemistry and material properties on degradation have been reported by Gross and coworkers.[32] Moreover, many other properties of PLACNs, such as the thermal stability, rheology, melting behavior, and mechanical properties have also been reported in the literature.[33–35] But, the effect of organic modifier on thermal and biodegradation behavior has not been studied. Moreover, the enzymatic degradation of polymer in the presence of nanoclay is still unexplored.

In this study, we report the preparation of PLA/layered silicate nanocomposites, with varying organic modification (15A and 30B nanoclay) and detailed studies about the nanostructure, crystal structure, morphology, and thermal properties. The biodegradation of PLA and its nanocomposites in different media such as compost and buffer solution has been studied. Finally, we report the enzymatic degradation of PLA nanocomposites and analyze the surface and bulk morphology of as prepared and degraded samples. The relative rate of biodegradation of PLA has been studied in the presence of different nanoclays. In addition, the effect of organic modification on biodegradation has been illustrated and compared with the possible reason through interactions between matrix polymer and nanoclay.

EXPERIMENTAL

Nanocomposite Preparation

PLA ($M_W = 1.7 \times 10^5$, PDI = 1.76) from Dow-Cargill, Minnesota, USA was used as received for this study. Two different types of organically modified nanoclays were used based on montmorillonite (Southern Clay, USA, CEC 110 meq/100 g), ion exchanged with methyl tallow *bis*-hydroxyethyl quaternary ammonium (Cloisite 30B) and dimethyl dihydrogenated tallow quaternary ammonium (Cloisite 15A). The chemical structures of PLA and organic modifiers are shown in Scheme 1. The organically modified nanoclay was sonicated in chloroform to achieve a good dispersion. The nanocomposites of PLA were prepared through solution route[34] by dissolving PLA (1 g) in the dispersion of nanoclay (40 mg) in chloroform, followed by removing the solvent by evaporation at a fast rate. The solution was stirred for 40 min to ensure proper mixing. Henceforth, we will term the pure organically modified clays as 15A and 30B and their corresponding nanocomposites as PLA-15A and PLA-30B, respectively. In both the cases, 4 wt % of nanoclays were used to prepare the nanocomposites. The films were dried over vacuum for 24 h.

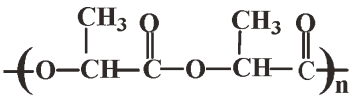

Polylactide

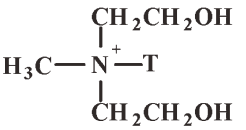

Methyl tallow bis-2-hydroxyethyl ammonium salt (30B)

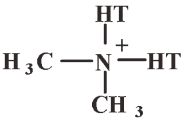

Dimethyl dihydrogenated tallow ammonium Salt (15A)

Scheme 1. The chemical structures of PLA and organic modifiers used in 30B and 15A nanoclays.

Characterization Techniques

X-Ray Diffraction. X-ray diffraction (XRD) experiments were performed using a Bruker AXS D8 Advance wide-angle X-ray diffractometer with Cu Kα radiation (wavelength, $\lambda = 0.154$ nm) and a graphite monochromator. The generator was operated at 40 kV and 20 mA. The thin sheet of the samples was placed on a quartz sample holder at room temperature and was scanned at diffraction angle 2θ from 1 to 40° at the scanning rate of 1°/min.

Thermal Characterization. Thermal behavior of freshly prepared nanocomposites and pure PLA films was investigated using a Mettler 832 DSC instrument. The samples were heated from 10 to 185°C at the scan rate of 10°C/min. The differential scanning calorimetry (DSC) was calibrated with indium and zinc before use. Thermogravimetric analyses were carried out using Mettler TGA, at a heating rate of 10°C/min from room temperature to 1000°C in nitrogen atmosphere both for pure polymer and for nanocomposites. PLA and its nanocomposites have been annealed in hot stage at 130°C for 2 h for DSC and XRD characterization.

Hardness Measurement. The shore A hardness tests were performed using a analog Shore A Hardness Tester, as per ASTM D2240 with rectangular thick sample sheet of 74.0 × 25.0 × 3.2 mm^3.

Morphological Investigation. The surface morphology of pure PLA and its nanocomposites was investigated by using both scanning electron microscope (SEM) and atomic force microscope (AFM). The surface morphology of the samples was examined with a LEO 435VP instrument operated at 10 kV. All the samples were gold coated by means of a sputtering apparatus before observation. AFM was performed using a NT-MDT multimode AFM, Russia, controlled by Solver scanning probe microscope controller. Tapping mode was used for surface morphology. The roughness of the surfaces caused by biodegradation was also examined by AFM measuring the height profile of the surface. The spherulitic morphology was examined by using

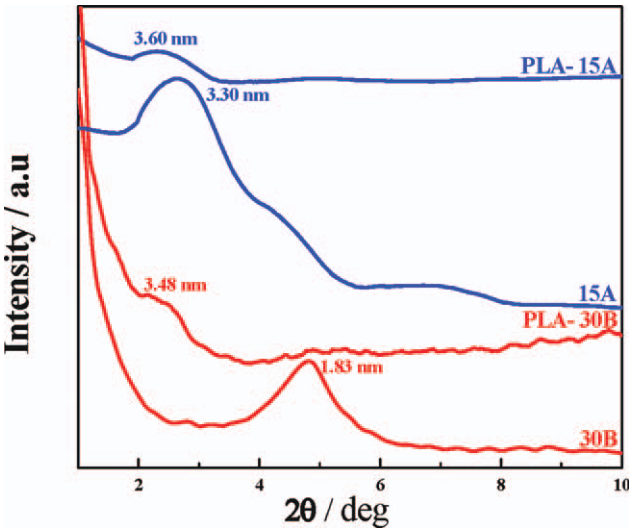

Figure 1. Wide-angle XRD patterns of organically modified nanoclays and PLA nanocomposites as indicated. The numbers in nanometer indicate the corresponding *d*-spacings.[Color figure can be viewed in the online issue, which is available at wileyonlinelibrary.com.]

a polarizing optical microscope (Leica) after crystallizing the samples at 130°C for 24 h on a Mettler hot stage. To observe the morphology of the PLA sheet and its nanocomposites in *Z*-section before and after enzymatic degradation, the samples were stained with *Rhodamine B* and scanned under Zeiss LSM 510 Meta laser scanning confocal microscope (LSCM). The stained samples were also observed under phase contrast microscope (Nikon eclipse E800).

Biodegradation Studies

Biodegradability of PLA and its nanocomposites was studied in a sealed chamber at constant humidity of ~85% and at 35°C.[5,22] Enzyme (Proteinase-k and Pseudomonas lipase type XIII), composted manure, and buffer solution were used as the biodegradation media. The initial dimensions of the samples were ~10 × 10 × 1 mm^3 for compost experiment and ~10 × 10 × 0.01 mm^3 for enzymatic studies. Comparative enzyme degradation was carried out in phosphate buffer medium (pH = 7.4).

Interactions Through Fourier Transform Infrared Spectroscopy

IR spectroscopy (Shimadzu, Japan) was employed to characterize the pure PLA and its nanocomposites. A thin film of the sample was characterized in transmittance mode. Fourier transform infrared (FTIR) spectra were obtained at wavenumber ranging from 400 to 4000 cm^{-1}.

RESULT AND DISCUSSION

Nanostructure

Figure 1 compares the XRD patterns of pure organoclays (15A and 30B) and their corresponding nanocomposites (PLA-15A and PLA-30B). A shift in the diffraction peak toward lower angle has been observed for nanocomposites as compared to pure nanoclays, suggesting intercalated nanostructure owing to the inclusion of polymer molecules inside the clay galleries.[22] Mean interplanar spacings, as calculated from Bragg's equation, of 15A and PLA-15A are 3.3 and 3.6 nm, respectively. On the other hand, the interplanar spacing of 30B nanoclay increases from 1.83 to 3.48 nm in nanocomposite, indicating intercalation of polymer chains within 30B-layered silicates. Two distinct levels of intercalation are evident from different organoclays and the extent of intercalation strongly depends on the nature of organic modifications. The favorable interactions between organic modifier and PLA chains dictate the degree of intercalation in two different types of organoclays. The hydroxyl group present in 30B organoclay interacts with carbonyl group in PLA chain which is mainly responsible for enhanced interaction, causing more intercalation of polymer chains in the gallery against the tallow and methyl groups present in 15A nanoclay. The crystallite size calculated from the Scherrer equation, $D_{hkl} = \kappa\lambda/\beta\cos\theta$, where κ is constant, λ is the wavelength of X-ray used, β is full-width at half-maxima, and θ is peak angle of (001) reflection which increases for nanocomposites (Table I), indicating interaction of polymer chain inside silicate galleries. The higher interaction in PLA-30B is also reflected in greater increase of D_{hkl} for PLA-30B as compared to PLA-15A.[22,16]

Structure

Figure 2(a) shows the XRD patterns of neat PLA and its nanocomposites after annealing. Quenched samples of PLA and its nanocomposites are predominantly amorphous [inset of Figure 2(a)] but after annealing PLA and nanocomposites become crystalline, showing four intense peaks at 2θ = 14.4, 16, 18.2, and 28.4° corresponding to (010), (110)/(200), (203), and (105) planes, respectively. But, those peaks are slightly shifted to lower angle in nanocomposites as compared to pristine PLA owing to the formation of imperfect crystals in the presence of nanoclay. However, orthorhombic crystalline structure of PLA is retained in the presence of nanoclay in nanocomposites but the peak

Table I. The Characteristics of Pure PLA, Nanoclays, and Their Nanocomposites

Sample	$M_W \times 10^{-5}$	d_{001} (nm)	D_{hkl} (nm)	T_d (°C) (5% wt. loss)	T_{ma}[a] (°C)	ΔH_{fb}[b] (J g^{-1})	ΔH_{fa}[c] (J g^{-1})	T_c (°C)	T_g (°C)	ΔH_c (J g^{-1})
PLA	1.7	-	-	340	150 ± 1	1.2	28 ± 2	63	57	7.2 ± 1
15A	-	3.34	14	-	-	-	-	-		-
PLA-15A	1.7	3.68	19	345	151 ± 0.5	1.1	27 ± 1	64	58	2.5 ± 2
30B	-	1.83	18	-	-	-	-	-		-
PLA-30B	1.7	3.7	29	350	152 ± 1	1.0	25 ± 0.5	64	58	2.5 ± 1

[a]T_{ma}, melting temperature after annealing., [b]ΔH_{fb}, heat of fusion before annealing., [c]ΔH_{fa}, heat of fusion after annealing.

Applied Polymer SCIENCE

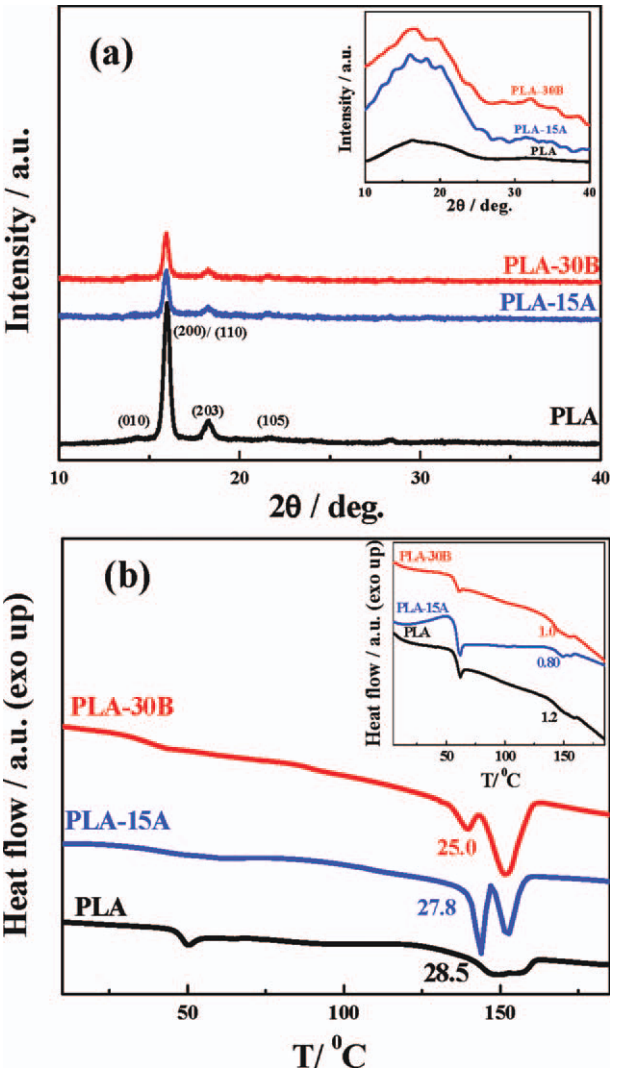

Figure 2. (a) XRD patterns of pure PLA and its indicated nanocomposites. The inset figures represent the XRD patterns for quenched samples, and (b) DSC thermograms of PLA and its indicated nanocomposites. The numbers indicate the heat of fusion in J/g and the inset figures there represent the DSC thermograms of quenched samples. [Color figure can be viewed in the online issue, which is available at wileyonlinelibrary.com.]

intensities have reduced *vis-à-vis* pristine PLA, indicating less crystallinity in nanocomposites owing to the above-mentioned interactions between nanoclay and polymer matrix.[25]

Thermal Properties

Thermal behavior of nanocomposites with the addition of two different types of organically modified nanoclays into polymer matrix is one of our interests. Figure 2(b) shows the DSC thermograms of pristine PLA and its nanocomposites after annealing [inset of Figure 2(b) shows the patterns before annealing]. The quenched samples exhibit distinct glass transition temperatures at ~58°C but the heats of fusion are minimal, indicating predominantly amorphous nature of quenched sample which was also evident from XRD patterns [Figure 2(a)]. After annealing, the double melting endotherms are prominent and heats of fusion become 28.5, 27.8, and 25.0 J g^{-1} for PLA, PLA-15A, and PLA-30B, respectively. The double-melting phenomena might be owing to melt recrystallization.[21] The Heat of fusion is a measure of interaction between the two components present in any composite/blend. The extent of interaction is more in PLA-30B as compared to PLA-15A nanocomposite as revealed from the lowest heat of fusion in PLA-30B owing to dipolar interaction between —*OH* group of organic modifier and ester group of PLA. However, crystallinity of PLA and its nanocomposites increases considerably after annealing as a result of crystallization during annealing above their glass transition temperature. The appearance of glass transition temperature for pure PLA and nanocomposites is also seen after annealing. Slight increase of crystallization temperatures for nanocomposites suggests the nucleating nature of nanoclays. Further, heats of crystallization also show a lower values (7.2, 2.5, and 2.5 J g^{-1} for PLA, PLA-15A, and PLA-30B, respectively) for nanocomposites. The nucleating phenomena have also been confirmed from the spherulite size of the crystallized samples (T_c = 130°C). The average spherulitic diameters are 180 ± 7, 175 ± 8, and 80 ± 5 μm for PLA, PLA-15A, and PLA-30B, respectively (Figure 3). The strong interaction restricts the spherulitic growth in nanocomposites as compared to pure PLA. Moreover, pristine PLA formed highly ordered and compact spherulites, whereas the nanocomposites exhibit less ordering and coarse spherulites owing to obstruction by the nanoclay in the crystal growth front during the growth of spherulites.[25]

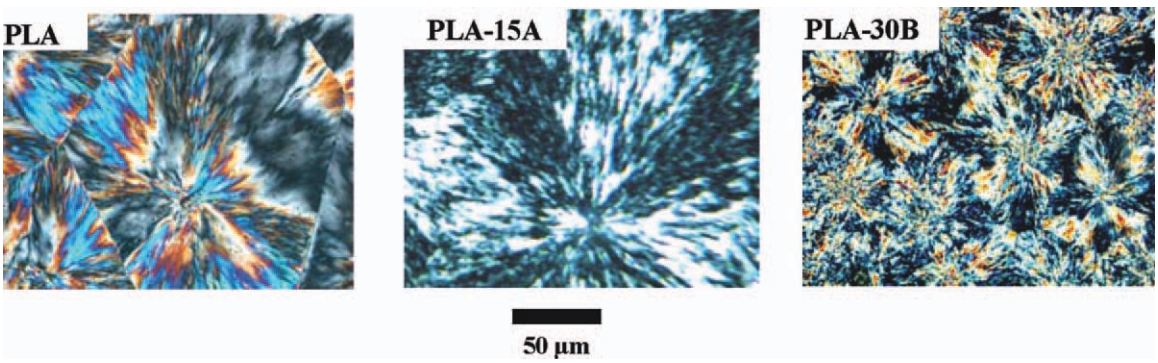

Figure 3. Polarizing optical micrographs of pure PLA and its indicated nanocomposites. The samples were crystallized at 130°C for 12 h. [Color figure can be viewed in the online issue, which is available at wileyonlinelibrary.com.]

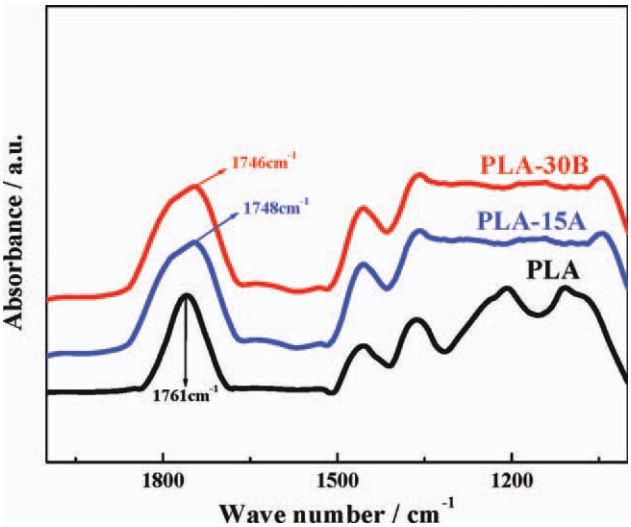

Figure 4. FTIR spectra of pure PLA and its indicated nanocomposites. [Color figure can be viewed in the online issue, which is available at wileyonlinelibrary.com.]

Thermogravimetric analyses for PLA and its nanocomposites (Supporting Information Figure S1) show that the decomposition temperature increases by 10°C with the addition of 4 wt % organically modified nanoclay (Table I). The inorganic nanoclay enhances the thermal performance by acting as a better mass transport barrier in the presence of disk-like inorganic nanoclay distributed uniformly in the polymer matrix.[36,37]

Mechanical Properties

Hardness Test. The hardness of pure PLA and its nanocomposites has been measured by using Shore A hardness tester. The hardness values are 90 ± 1, 92 ± 0.5, and 95 ± 2 for pure PLA, PLA-15A, and PLA-30B, respectively. Hence, the hardness of nanocomposites increases in the presence of nanoclays in nanocomposites and the increment is slightly more in PLA-30B as compared to PLA-15A as a result of better distribution of nanoclay owing to enhanced interaction. Similar enhancement of hardness in the presence of nanoclay has been observed for other polymers.[38,39]

Interaction in Nanocomposites. In the previous sections, we have noticed that the enhancement of properties strongly depends on the type of organic modifications used. FTIR studies have been performed to know the type of interactions occurred between matrix polymer and organically modified nanoclays (Figure 4). The shift of $>C{-}O$ stretching frequency of PLA nanocomposites toward lower wave number (PLA-30B at 1746 cm^{-1} and for PLA-15A at 1748 cm^{-1}) against pure PLA at 1761 cm^{-1} has been observed. Further, the relative shifting is more for PLA-30B as compared to PLA-15A, indicating stronger interaction with 30B nanoclay.

The quantitative estimation of interaction parameter has been carried out through melting point depression technique. The extrapolation technique of $T_m - T_c$ plot to the $T_m = T_c$ line (Hoffman–Weeks plot) has been used to measure the equilibrium melting point. Figure 5(a) shows the representative plot of melting point against heat of fusion of pure PLA crystallized at different temperatures mentioned for various time. The melting temperature correspond to 5% heat of fusion (ΔH) has been taken into account to calculate the T_m in that particular crystallization temperature (T_c). The melting point increases with increasing crystallization temperature (T_c) and this phenomenon is also followed for nanocomposites. The $T_m - T_c$ plot is shown in Figure 5(b) in which the melting points of the nanocomposites are slightly lower than that of pure PLA for any particular T_c.[40] The equilibrium melting points, T_m^0 of pure PLA and its nanocomposite (representative PLA-30B) have been calculated after extrapolation of $T_m - T_c$ plot to $T_m = T_c$ line and the values are 172 and 162°C for neat PLA and PLA-30B, respectively. The equilibrium melting temperature of the nanocomposites decreases as a result of interaction between matrix polymer and organically modified clays.[40] The sufficient negative value of the interaction parameter (χ) = -2.35×10^{-5} (as calculated from the equation below of Nishi and Wang)

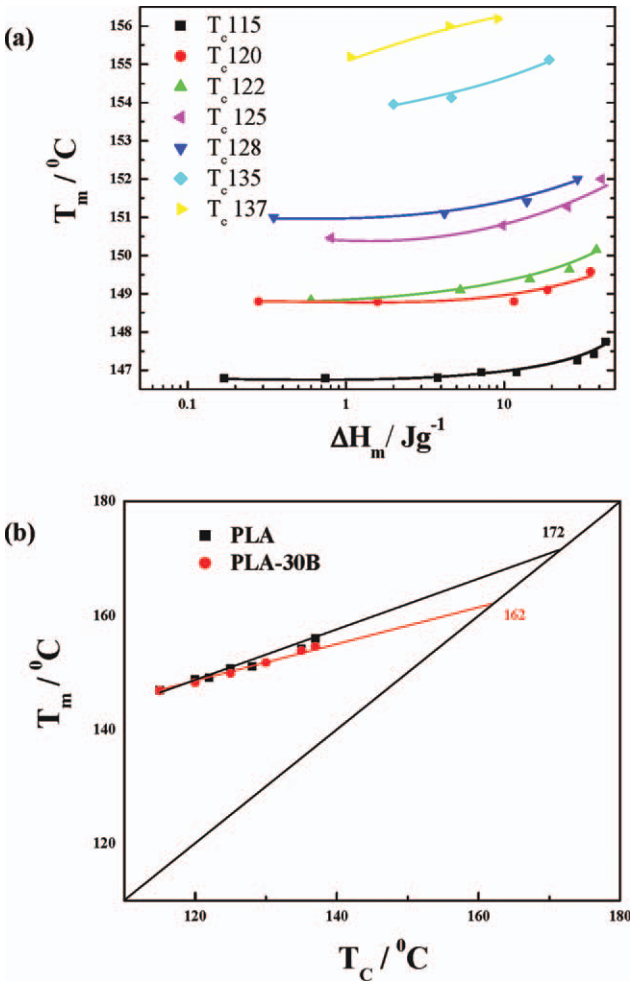

Figure 5. (a) Representative plot of melting temperatures (T_m) versus. heat of fusion (ΔH) of pure PLA at the indicated crystallization temperatures (T_c). (b) $T_m - T_c$ plot at 5% ΔH for indicated specimens. The numbers show the corresponding equilibrium melting temperatures in °C. [Color figure can be viewed in the online issue, which is available at wileyonlinelibrary.com.]

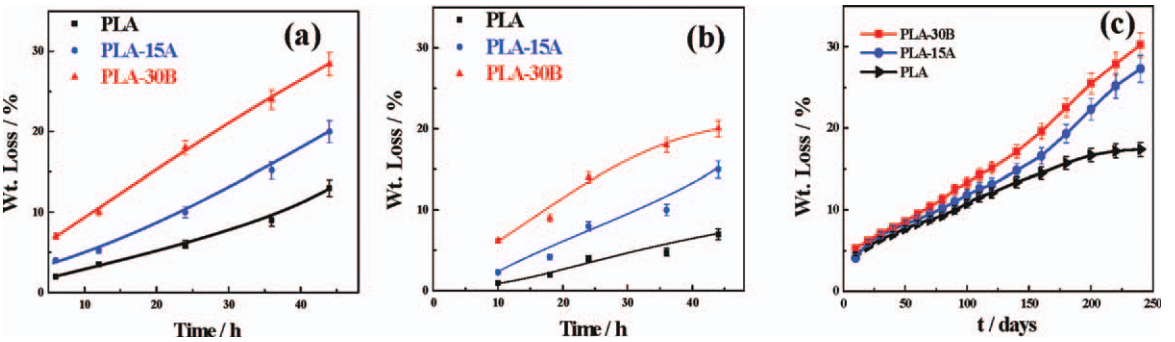

Figure 6. Percentage weight loss of PLA and its indicated nanocomposites during enzymatic ((a) in Proteinase-k (b) in Lipase from Pseudomonas sp., Type XIII) degradation at 37°C. (c) In compost media. [Color figure can be viewed in the online issue, which is available at wileyonlinelibrary.com.]

indicates strong interaction between 30B nanoclay and PLA matrix.[40,41]

$$\frac{1}{T^o_{NC}} - \frac{1}{T^o_{PLA}} = -\frac{RV_{PLA}}{\Delta H_u V_{clay}} \phi^2_{clay} \chi$$

where T^o_{NC} and T_{PLA} are the equilibrium melting points of the nanocomposite and that of the pure PLA, respectively. V_{PLA} and V_{clay} are the molar volumes of the repeating unit of PLA and the molar volume organoclay, respectively, ϕ_{clay} is the volume fraction of clay, and ΔH_u is the enthalpy of fusion per mole of repeating unit of PLA. The similar measurement of calculating interaction parameter was adopted for polymer blend systems[41,42] using melting point depression technique. Hence, both the FTIR and the χ-measurements confirm the strong interaction in nanocomposites and relatively PLA-30B system exhibits stronger interaction as evident from lowering of FTIR peak.

Biodegradation. The enzymatic degradation rates of nanocomposites are much faster than that of pure PLA [Figure 6(a,b)] and among the nanocomposites, PLA-30B exhibits higher degradation rate as compared to PLA-15A. The matrix polymer degrades at a higher rate in the presence of organically modified nanoclay raising a clay dependency phenomenon. Figure 6(a,b) also shows that the enzymatic degradation is higher with *Proteinase-k* as compared to Lipase: type XIII from Pseudomonas sp. Hence, it is concluded that *Proteinase-k* is more effective for PLA degradation as compared to Lipase: type XIII from Pseudomonas sp. Several reports of enzymatic degradation of pure PLA by *Proteinase-k* have been accounted and the report is in agreement with our experimental results.[43,44] The bulk morphology in *Z*-section as observed in scanning confocal images before and after degradation exhibits highest enzymatic degradation in PLA-30B and lowest in pure PLA [(Figure 7(a)]. Smooth bulk morphologies have been observed before enzymatic degradation, whereas distinct pittings have been noticed after degradation whose relative measure shows maxima in PLA-30B.

The phase contrast images of the surface of pristine PLA and its nanocomposites (before and after enzymatic degradation) also indicate the relative degradation rate PLA-30B > PLA-15A > PLA of pure polymer and different nanocomposites [Figure 7(b)]. Hence, both the surface and the bulk morphologies confirm the varying degradation rates of pure polymer and nanocomposites with two different nanoclays. The changes in weight loss owing to biodegradation in compost manure are shown in Figure 6(c). The rate of biodegradation is quite slow for pristine PLA (maximum 17% weight loss in 240 days). On the other hand, the biodegradation rate has enhanced significantly in nanocomposites in the presence of nanoclays with 27 and 31 wt % loss observed in the same time for PLA-15A and PLA-30B, respectively. Biodegradation/weight loss of matrix PLA is a result of hydrolytic cleavage of ester bond by specific enzyme.[45] However, biodegradation rate is quite slow in compost as compared to pure enzyme (Proteinase-k, Lipase from Pseudomonas sp., type XIII), presumably owing to lower concentration of specific enzyme necessary to hydrolyze PLA present in compost. Hence, the biodegradation rate is highly dependent on the media used. The presence of specific microorganism which secretes particular depolymerase is necessary for biodegradation of PLA and its nanocomposites. Higher biodegradation rate of PLA-30B is primarily owing to the greater interaction between PLA and 30B nanoclay and better dispersion of nanoparticles in matrix polymer, as evident from the lower heat of fusion and XRD analysis. Better interaction lead to an increase of amorphous zone. Higher the amorphous zone, more susceptible is the hydrolysis by microorganism for degradation of the polymer. In addition, the presence of excess hydroxyl groups in the organic modifier of 30B nanoclay and the presence of terminal hydroxylated edge groups of the silicate[28] may accelerate the hydrolytic decomposition responsible for higher biodegradation of PLA in the presence of 30B clay.

Higher biodegradation rate of PLA-30B nanocomposites as compared to PLA-15A is presumably owing to the greater interaction between PLA and 30B nanoclay and better dispersion of nanoparticles in matrix, as evident from the lower heat of fusion and XRD analysis as compared to PLA-15A nanocomposites.[46,47] In addition, the presence of excess hydroxyl groups in the organic modifier of 30B nanoclay may accelerate the hydrolytic decomposition against 15A nanoclay, where methyl and hydrogenated tallow groups are at hand in organic modifier. The surface roughening owing to biodegradation in compost media has been shown by using SEM micrographs of pure PLA and its nanocomposites (PLA-15A and PLA-30B) in compost manure [Figure 8(a)].

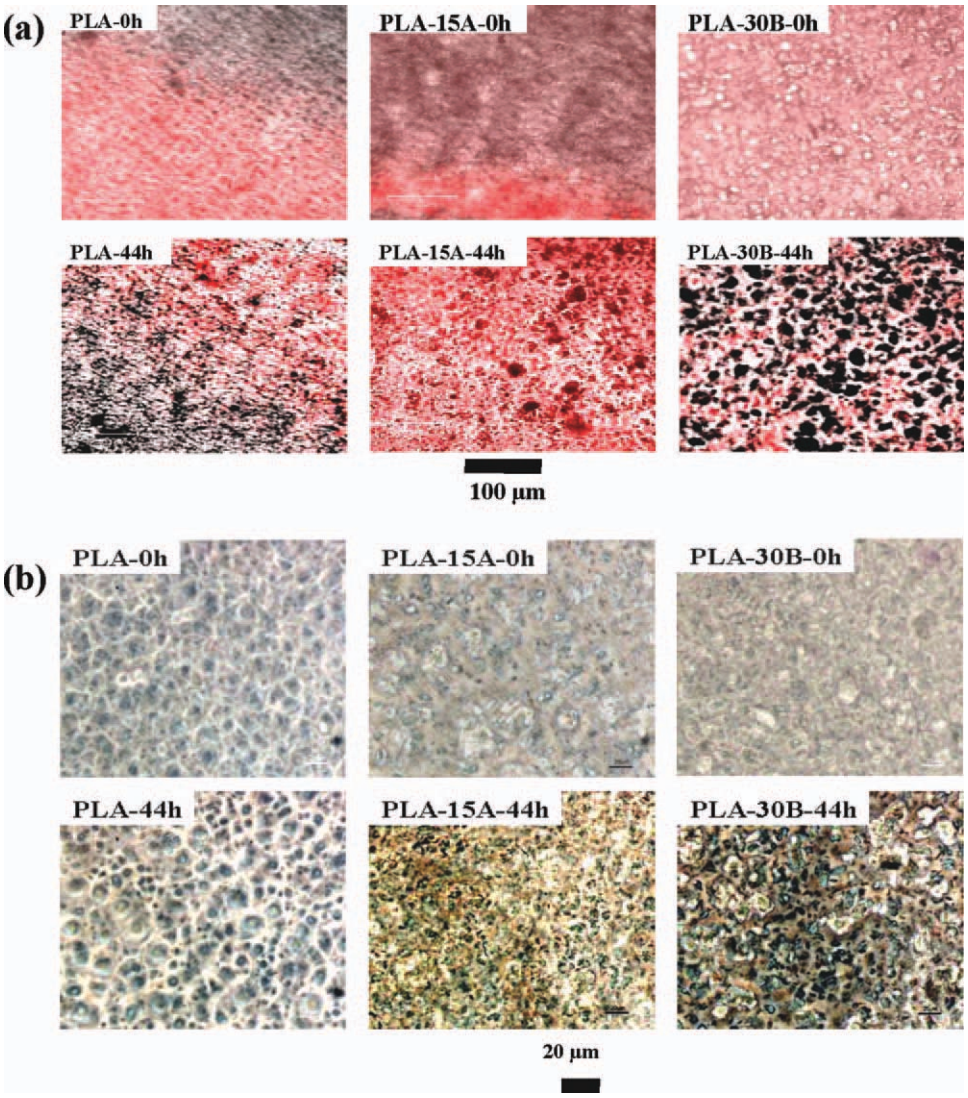

Figure 7. (a) LSCM image (b) phase contrast images of PLA and its indicated nanocomposites. The numbers after the specimens name represent the biodegradation time in hours. The number "0" indicates the sample before starting enzymatic degradation. [Color figure can be viewed in the online issue, which is available at wileyonlinelibrary.com.]

The greater loss of samples from the surfaces occurred in nanocomposites as bigger pits are observed as compared to pristine PLA. Furthermore, the pitting appeared in excess in PLA-30B than that of PLA-15A nanocomposite for the same time of exposure (240 days). Both PLA and its nanocomposites do not exhibit any pitting before biodegradation. Hence, surface roughening occurred in greater extent in nanocomposites owing to enhanced biodegradation with respect to pristine PLA. Figure 8(b) shows the AFM images of samples before and after biodegradation.[16,40] The granular morphology of PLA and its nanocomposites is evident before soil burial, whereas roughening is observed after biodegradation. The nanocomposites experience greater coarsening as compared to pristine PLA. Height profiles obtained from the AFM topographs show comparatively smooth surface before degradation for both pure PLA and nanocomposites, whereas roughening of surface has been noticed quantitatively after biodegradation (Figure 9). In addition, the relative roughness for PLA-30B is more in comparison to PLA-15A as evident from the right-side height profiles. To show the biodegradation mechanism, we conducted the DSC experiment before and after biodegradation. Figure 10 shows the heat of fusion of pristine PLA and its nanocomposites as a function of biodegradation time. Before starting biodegradation, the samples reveal almost same and very low ΔH, whereas with increasing biodegradation time ΔH has significantly been enhanced. With biodegradation time, the amorphous content of the samples has gradually been consumed up by the microorganism, keeping more the crystalline component in the remaining samples which exhibit higher heat of fusion. Moreover, PLA-30B system shows higher ΔH as compared to PLA-15A system as the extent of biodegradation is more in PLA-30B, causing greater loss of amorphous part from the sample during biodegradation.

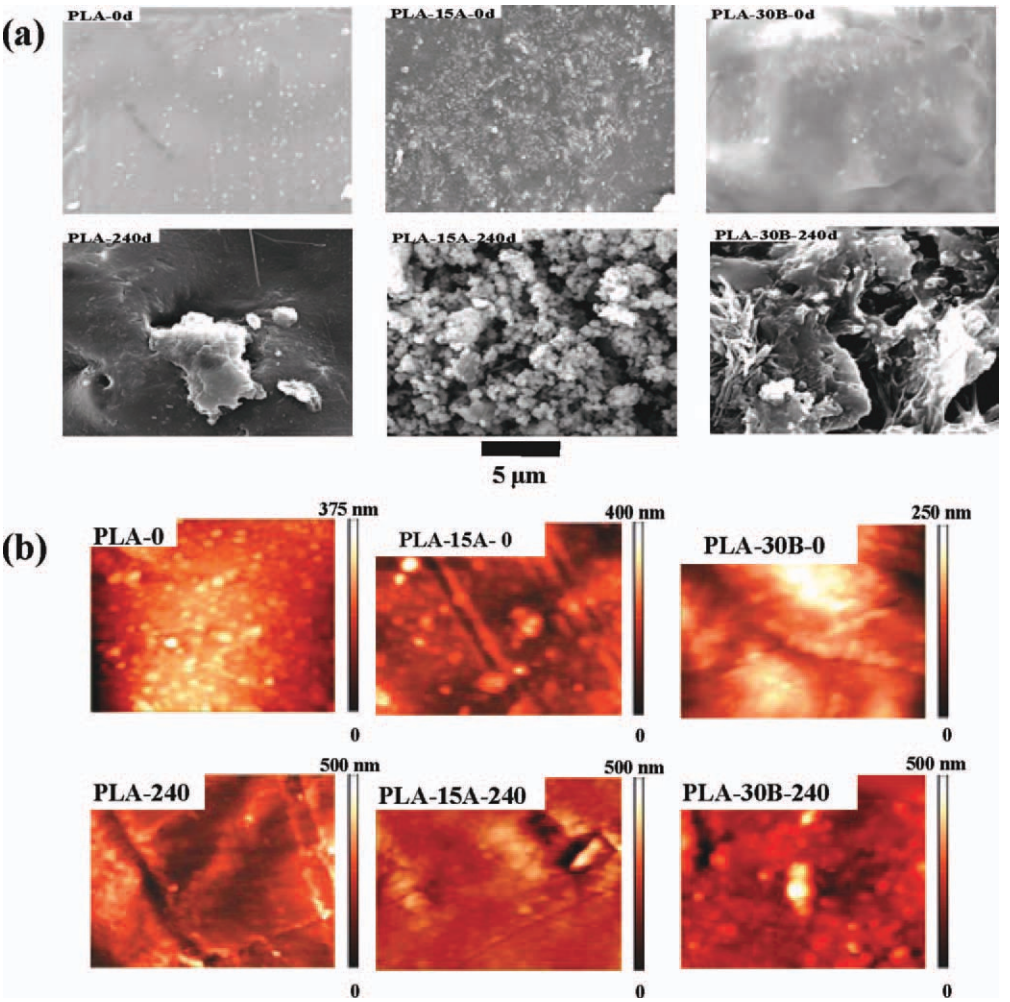

Figure 8. (a) FE-SEM images (b) AFM images of representative pristine PLA and its nanocomposite before and after compost degradation. The numbers after the specimens name represent the biodegradation time in day for compost degradation. [Color figure can be viewed in the online issue, which is available at wileyonlinelibrary.com.]

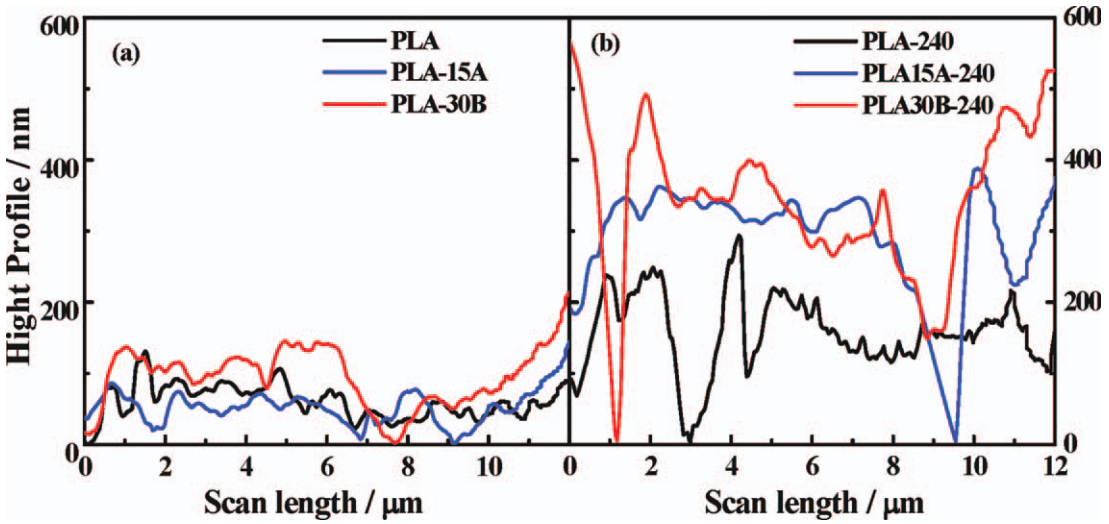

Figure 9. Height profile of PLA and its indicated nanocomposites (a) before (left side) and (b) after (right side) degradation in compost media. The number after the sample indicates the degradation time in days. [Color figure can be viewed in the online issue, which is available at wileyonlinelibrary.com.]

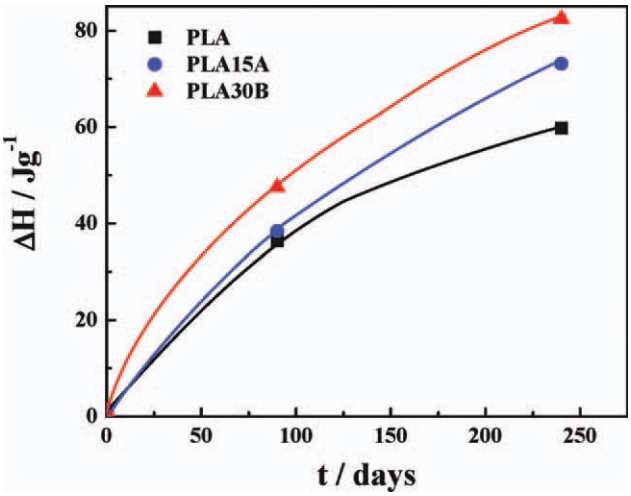

Figure 10. Heat of fusion as a function of biodegradation time for pure PLA and its indicated nanocomposites. [Color figure can be viewed in the online issue, which is available at wileyonlinelibrary.com.]

CONCLUSIONS

PLA/layered silicate nanocomposites have been prepared through solution route using two different types of organoclays. The nature of organic modifiers present in layered silicate has markedly influenced the properties of the nanocomposites. Both organically modified nanoclays 15A and 30B form intercalated nanocomposites and the extent of intercalation is much higher in PLA-30B nanocomposites because of greater interaction between the components. The orthorhombic crystal structure of PLA is retained in the presence of nanoclays. Melt-quenched PLA and its nanocomposites are predominantly amorphous, whereas annealing improves their crystallinity. Nanoclays act as nucleating agents as evident from lowering of spherulitic dimension for nanocomposites as compared to neat PLA. The presence of nanoclay has increased the rate of biodegradation in PLA and its extent depends on the type of nanoclays used. The rate of biodegradation is high again in enzymatic media as compared to compost for similar set of samples. Morphologies confirm the extent of biodegradation rate is higher in nanocomposites as compared to pure PLA and relative rate is higher in PLA-30B nanocomposite as compared to PLA-15A system. The amorphous zones are biodegraded first *vis-à-vis* the crystalline region as evident from the steep increase of heat of fusion with biodegradation time.

ACKNOWLEDGMENTS

The authors acknowledge the receipt of research funding from Department of Biotechnology (DBT), New Delhi, Ministry of Science and Technology, Government of India (Project No. *BT/PR-6929/BCE/08/433/2005*). The national facility of Scanning Confoacl Microscopy under Prof. S. C. Lakhotia and Prof. J. K. Roy, supported by *DST*, India, is also gratefully acknowledged.

REFERENCES

1. Tanaka, Y.; Yamaoka, H.; Nishizawa, S.; Nagata, S.; Ogasawara, T.; Asawa Y.; Fujihara, Y.; Takato, T.; Hoshi, K. *Biomaterials* **2010,** *31*, 4506.
2. Francois, S.; Chakfé', N.; Durand, B.; Laroche, G. *Acta Biomater.* **2009,** *5*, 2418.
3. Drumright, R. E.; Gruber, P. R.; Henton, D. E. *Adv Mater.* **2000,** *12*, 1841.
4. Iwata, T.; Doi, Y. *Macromolecules* **1998,** *31*, 2461.
5. Maria, A.; Cristina, A; Kikku, F; Mara, G. *Environ. Sci. Pollut. Res.* **2011,** *18*, 865.
6. Fukushima, K.; Abbate, C.; Tabuani, D.; Gennari, M.; Camino, G. *Polym. Degrad. Stab.* **2009,** *94*, 1646.
7. Nieddu, E; Mazzucco, L.; Gentile, P.; Benko, T.; Balbo, V.; Mandrile, R; Ciardelli, G. *React. Funct. Polym.* **2009,** *69*, 371.
8. Singh, N. K.; Purkayastha, B. P. D.; Roy, J. K.; Banik, R. M.; Gonugunta, P.; Misra, M.; Maiti, P. *J. Mater. Chem.* **2011,** *21*, 15919.
9. Mikos, A. G.; Lyman, M. D.; Freed, L. E.; Langer, R. *Biomaterials* **1994,** *15*, 55.
10. Kamath, K. R.; Park, K. *Adv. Drug Deliv. Rev.* **1993,** *11*, 59.
11. Kricheldorf, H. R.; Berl, M.; Scharngal, N. *Macromolecules* **1988,** *21*, 286.
12. LeBaron, P. C.; Wang, Z.; Pinnavaia, T. *J. Appl. Clay Sci.* **1999,** *15*, 11.
13. Giannelis, E. P. *Adv. Mater.* **1996,** *8*, 29.
14. Maiti, P.; Nam, P. H., Okamoto, M., Hasegawa, N.; Usuki, A. *Macromolecules* **2002,** *35*, 2042.
15. Shah, D.; Maiti, P.; Jiang, D.; Giannelis, E. P. *Adv. Mater.* **2005,** *17*, 525.
16. Maiti, P.; Yadav, P. J. P. *J. Nanosci. Nanotechnol.* **2008,** *8*, 1858.
17. Marras, S. I.; Zuburtikudis I.; Panayiotou, C. *Eur. Polym. J.* **2007,** *43*, 2191.
18. Kim, H. S.; Park, B. H.; Yoon, J.; Jin, H. *Eur. Polym. J.* **2007,** *43*, 1729.
19. Gestí, S.; Zanetti, M.; Lazzari, M.; Franco, L.; Puiggalí, J. *Eur. Polym. J.* **2009,** *45*, 398.
20. Lagaly, G. *Appl. Clay Sci.* **1999,** *15*, 1.
21. Maiti, P.; Yamada, K.; Okamoto, M.; Ueda, K.; Okamoto, K. *Chem. Mater.* **2002,** *14*, 4654.
22. Ray, S. S.; Maiti, P. Okamoto, M.; Yamada, K.; Ueda, K. *Macromolecules* **2002,** *35*, 3104.
23. Ray, S. S.; Yamada, K.; Okamoto, M.; Fujimoto, Y.; Ogami, A.; Ueda, K. *Polymer* **2003,** *44*, 6633.
24. Ray, S. S.; Yamada, K.; Okamoto, M.; Ogami, A.; Ueda, K. *Chem. Mater.* **2003,** *15*, 1456.
25. Nam, J. Y.; Ray, S. S.; Okamoto, M. *Macromolecules* **2003,** *36*, 7126.
26. Nam, P. H; Kaneko, M.; Ninomiya, N.; Fujimori, A.; Masuko, T. *Polym. Int.* **2006,** *55*, 916.
27. Nam, P. H.; Kaneko, M.; Ninomiya, N.; Fujimori, A.; Masuko, T. *Polymer* **2005,** *46*, 7403.
28. Ray, S. S.; Yamada, K.; Okamoto, M.; Ueda, K. *Nano. Lett.* **2002,** *2*, 1093.

29. Zheng, X.; Zhou, S.; Li, X.; Weng, J. *Biomaterials* **2006,** *27*, 4288.

30. Kunou, N.; Ogura, Y.; Hashizoe, M.; Honda, Y.; Hyon, S.; Ikada, Y. J. *Controlled Release* **1995,** *37*, 143.

31. Deng, X.; Hao, J.; Wang, C. *Biomaterials* **2001,** *22*, 2867.

32. MacDonald, R. T.; McCarthy, S. P.; Gross, R. A. *Macromolecules* **1996,** *29*, 7356.

33. Paul, M.; Alexandre, A. M.; Degee, P.; Calberg, C.; Jerome, R.; Dubois, P. *Macromol. Rapid Commun.* **2003,** *24*, 561.

34. Chang, J. H.; An, Y. U.; Sur, G. S. *J. Polym. Sci. B Polym. Phys.* **2003,** *41*, 94.

35. Ogata, N.; Jimenez, G.; Kawai, H.; Ogihara, T. *J. Polym. Sci. B Polym. Phys.* **1997,** *35*, 389.

36. Lim, S. T.; Hyun, Y. H.; Choi, H. J.; Jhon, M. S. *Chem. Mater.* **2002,** *14*, 1839.

37. Zhu, J.; Morgan, A. B.; Lamelas, F. J.; Wilkie, C. A. *Chem. Mater.* **2001,** *13*, 3774.

38. Kim, B. K.; Seo, J. W.; Jeong, H. M. *Eur. Polym. J.* **2003,** *39*, 85.

39. Ratnam, C. T.; Zaman, K. *Polym. Degrad. Stab.* **1999,** *65*, 99.

40. Singh, N. K.; Purkayastha, B. D.; Roy, J. K.; Banik, R. M.; Yashpal, M.; Singh, G.; Malik, S.; Maiti, P. *ACS Appl. Mater. Interfaces* **2010,** *2*, 69.

41. Maiti, P.; Nandi, A. K. *Macromolecules* **1995,** *28*, 8511.

42. Maiti, P.; Chatterjee, J.; Rana, D.; Nandi, A. K. *Polymer* **1993,** *34*, 4273.

43. MacDonald, R. T.; McCarthy S. P.; Gross, R. A. *Macromolecules* **1996,** *29*, 7356.

44. Kikkawa, Y. Suzuki, T.; Kanesato, M.; Doi, Y.; Abe, H. *Biomacromolecules* **2009,** *10*, 1013.

45. Murphy, C. A.; Cameron, J. A.; Huang, S. J.; Vinopal, R. T. *Appl. Environ. Microb.* **1996,** *62*, 456.

46. Maiti, P.; Batt, C. A.; Giannelis, E. P. *Biomacromolecules* **2007,** *8*, 3393.

47. Singh, N. K.; Banik, R. M.; Kulriya, P. K.; Awasthi, D. K.; Malik, S.; Maiti, P. *Nanosci. Nanotechnol. Lett.* **2009,** *1*, 52.